Microscopic and Nanoscopic Three-Phase-Boundaries of Platinum Thin-Film Electrodes on YSZ Electrolyte

Thomas Ryll, Henning Galinski, Lukas Schlagenhauf, Pierre Elser, Jennifer L. M. Rupp, Anja Bieberle-Hutter, and Ludwig J. Gauckler**

Agglomerated Pt thin films have been proposed as electrodes for electrochemical devices like micro-solid oxide fuel cells (μ-SOFCs) operating at low temperatures. However, comprehensive studies elucidating the interplay between agglomeration state and electrochemical properties are lacking. In this contribution the electrochemical performance of agglomerated and "dense" Pt thin film electrodes on yttria-stabilized-zirconia (YSZ) is correlated with their microstructural characteristics. Besides the microscopically measurable triple-phase-boundary (tpb) where Pt, YSZ and air are in contact, a considerable contribution of "nanoscopic" tpbs to the electrode conductivity resulting from oxygen permeable grain boundaries is identified. It is demonstrated that "dense" Pt thin films are excellent electrodes provided their grain size and thickness are in the nanometer range. The results disprove the prevailing idea that the performance of Pt thin film electrodes results from microscopic and geometrically measurable tpbs only.

1. Introduction

Thin Pt electrodes deposited on yttria-stabilized zirconia (YSZ) are one of the basic electrode-electrolyte systems in solid-state electrochemistry.[1–3] The performance of thin Pt electrodes is of practical importance for the development and miniaturization of devices like oxygen sensors[4] and solid oxide fuel cells (SOFCs).[5] On Pt electrodes, the electrochemical reaction is confined to the three-phase-boundary (tpb) where gas, electrolyte and electrode are in contact.[6] As it is generally accepted that oxygen transport does not occur through the grain interior of thin Pt films, a high tpb-length coexisting with two-dimensional percolation is considered crucial for the functionality of Pt electrodes on YSZ.

Percolating Pt networks with high tpb-length are obtained by annealing of Pt thin films initially deposited at low temperatures. The underlying kinetic process is termed thin film agglomeration or dewetting.[7] It is caused by the inherent thermodynamic instability of metal thin films on oxidic substrates, which becomes manifest in a negative difference of free energy per unit area comparing a dense metal film and isolated metal particles on an oxide surface.[8] Triggered by a decrease of free energy, dense metal films transform into isolated particles at elevated temperatures. The morphological changes of thin films during agglomeration can be subdivided into hole formation, hole growth and particle growth.[7] The latter step commences after the breakdown of a two-dimensionally percolating network. Thin film agglomeration is governed by the available diffusion mechanisms of the metal film and, therefore, accelerates with increasing temperature. Due to the increasing amount of film material to be transported, an increase of film thickness results in a slower progression of the agglomeration process. A model relating the hole radius during hole growth to time, temperature and film thickness has been established by Brandon and Bradshaw.[9]

At present, studies utilizing agglomerated Pt thin films on YSZ can be classified into two categories: (i) studies investigating the basic characteristics of Pt | YSZ electrodes such as the correlation of electrode polarization with oxygen partial pressure[10–12] and (ii) studies reporting on the application of agglomerated Pt films on thin YSZ electrolytes in electrochemical devices such as micro-SOFCs.[13–15]

Within basic studies, (i), tpb-lengths of up to 15 μm^{-1} have been reported for agglomerated Pt films on polycrystalline YSZ.[10] Furthermore, an inverse correlation of area specific resistance (ASR) with the microscopic and geometrically measurable tpb-length of agglomerated or micro-patterned Pt electrodes was found.[10,16] This correlation provides guidance for the fabrication of Pt thin film electrodes. However, as the authors kept the processing conditions of the Pt thin films largely constant, it remains unclear to what extend microstructural features like grain boundaries, triple lines as well as voids and grooves in the nanometer range contribute to the electrode conductance of Pt thin films. These features vary greatly depending on the deposition and annealing conditions of thin Pt films as well as on the underlying substrate.

For agglomerated Pt electrodes applied on thin YSZ electrolytes in micro-SOFCs, (ii), the available data is limited to power densities and electrode performances characterized by the ASR. Muecke et al. reported a power density of 5 mW cm^{-2} and an electrode ASR of 54 Ωcm^2 at 500 °C for a micro-SOFC composed of 35- to 50-nm thick agglomerated Pt electrodes deposited by sputtering and a YSZ thin film electrolyte.[13] Huang et al. deposited

T. Ryll, H. Galinski, L. Schlagenhauf, P. Elser, Dr. J. L. M. Rupp, Dr. A. Bieberle-Hutter, Prof. L. J. Gauckler
ETH Zurich, Department of Materials
Wolfgang-Pauli-Str. 10, 8093 Zurich, Switzerland
E-mail: thomas.ryll@mat.ethz.ch; ludwig.gauckler@mat.ethz.ch

DOI: 10.1002/adfm.201001729

80-nm thick Pt electrodes by sputtering on a 50-nm thick YSZ electrolyte film.[14] These cells exhibited a power density of 200 mW cm^{-2} and an electrode ASR as low as 30 Ω cm^2 at 350 °C. Latter value is surprisingly low in light of the fact that these films were not structured in any way in order to create a microscopic tpb. One can conclude that the cell performance of micro-SOFCs consisting of Pt electrodes and a thin YSZ electrolyte varies strongly. As the biggest losses in micro-SOFCs trace back to the electrodes, these variations indicate, that the choice of processing conditions and the agglomeration state significantly affect the conductance of thin Pt electrodes.

Despite the increasing use of agglomerated Pt thin films as electrodes, a comprehensive survey of the morphological evolution of Pt thin films on YSZ during agglomeration as a function of film thickness, microstructure, substrate properties and deposition conditions is lacking. It remains unclear to what extend the corresponding change of the tpb-length can be used to optimize the electrochemical performance of agglomerated Pt electrodes and, correspondingly, whether even better micro-SOFC performances are feasible by an optimization of the electrode morphology.

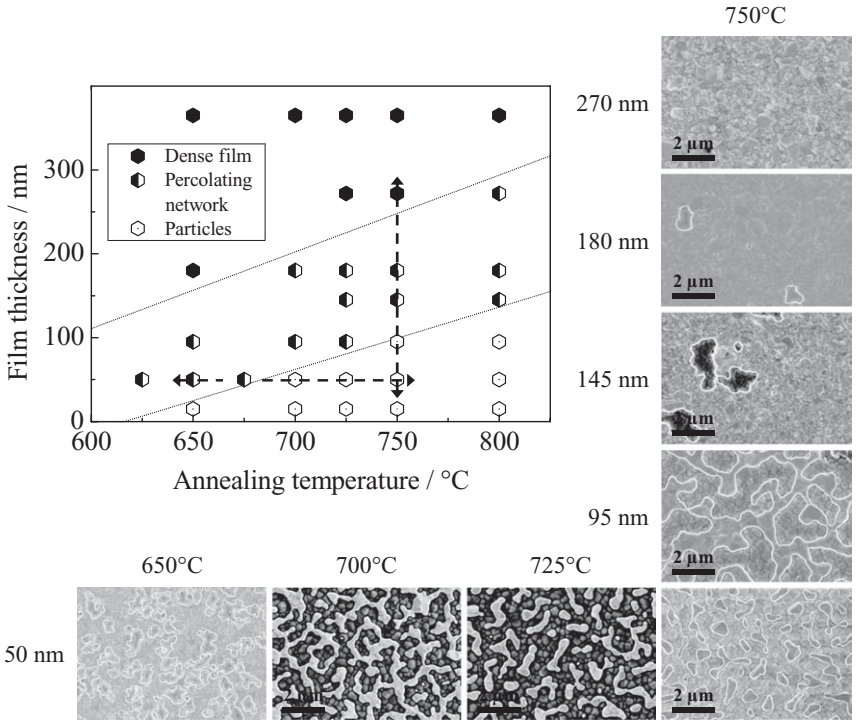

Figure 1. Morphological evolution of thin Pt films on YSZ tape caused by isothermal heat treatment for 2 h with respect to film thickness and temperature. Exemplary SEM top-view images are shown. Structures highlighted in grey feature a porous but two-dimensionally percolating Pt network. All films were deposited in 27 µbar of Ar using a plasma power of 360 W.

This study aims at a systematic investigation of Pt thin film agglomeration on polycrystalline YSZ with respect to film thickness and annealing temperature. Special attention is paid to the evolution of the geometrically measurable tpb-length per electrode area and its correlation with the ASR of agglomerated Pt electrodes. Furthermore, the electrochemical performance of agglomerated Pt thin films is compared to as-deposited and dense films. Based on the experimental results we discuss the role of "nanoscopic" tpbs, provided by microstructural features like grain boundaries and the geometrically measurable "microscopic" tpb of agglomerated Pt thin films on the overall electrode conductance. Finally, conclusions for high-performing Pt electrodes on YSZ electrolytes are drawn.

2. Results and Discussion

2.1. The Correlation of Microscopic tpb-length and Electrode Performance in the Case of Agglomerated Pt Films

In **Figure 1**, the morphologies of Pt films after annealing for 2 h are summarized with respect to film thickness and annealing temperature. Dense films, two-dimensionally percolating Pt networks and isolated Pt particles are specified by filled, partially filled and open symbols, respectively. Two datasets are exemplified by means of SEM top-view images: The horizontally arranged set of images illustrates the impact of annealing temperature on 50-nm thick Pt films, whereas the vertically arranged images depict the resulting morphologies of films with different thicknesses after annealing them all at 750 °C. It is found that the agglomeration process after annealing for 2 h is more advanced the thinner the films are and the higher the annealing temperature is. For the application of Pt electrodes at the interface between a gas and a solid electrolyte a percolating network as well as a high hole density are required. While the percolating network enables the transport of electrical current, the holes feature the tpb where the electrode reaction takes place. In Figure 1 film morphologies meeting this requirement have been highlighted in grey. Accordingly, the upper border of the grey-shaded area separates dense Pt films from two-dimensionally percolating Pt networks. The lower border designates the transition from percolating Pt networks to isolated Pt particles on the YSZ surface. The breakdown of two-dimensionally percolating networks was found to occur in the range of 48% to 55% of uncovered substrate area. This observation corresponds well with literature reporting an experimentally determined critical uncovered area of 37% to 48% for Pt on stabilized zirconia[17] and 40% to 50% estimated on the basis of Monte-Carlo studies.[18]

The performance of Pt electrodes is believed to correlate with the tpb-length. For this reason the microscopic tpb-length per electrode area was determined by SEM image analysis and is plotted over the percentage of uncovered substrate area for three film thicknesses in **Figure 2**. The data area corresponding to films featuring a percolating network is highlighted in grey. For the 50- and 95-nm thick Pt films a maximum tpb-length per electrode area was reached around 50% of uncovered

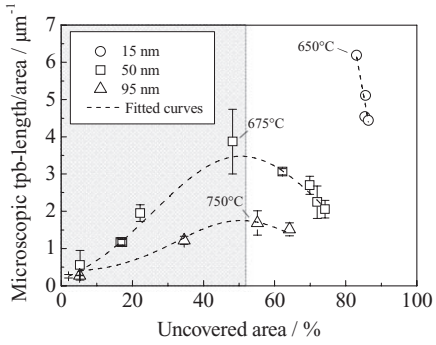

Figure 2. Development of the microscopic three-phase-boundary-length (tpb-length) per electrode area with increasing uncovered substrate area during the agglomeration of thin Pt films on YSZ tape. The fits are guide to the eye. Structures highlighted in grey feature a porous but two-dimensionally percolating Pt network.

substrate area. While the maximum tpb-length was 3.9 μm^{-1} for the 50-nm thick Pt films, only 1.7 μm^{-1} were obtained for the thicker films (95 nm). All 15-nm thick Pt films exhibited non-percolating morphologies above 80% of uncovered substrate area beyond the maximum tpb-length. Their tpb-lengths in the range of 4.4 to 6.2 μm^{-1}, which decrease with increasing uncovered substrate area, predict a maximum tpb-length way above the maximum tpb-length for 50-nm thick films.

The following conclusions can be drawn from the experimental data: Firstly, the maximum tpb-length obtained around 50% of uncovered substrate area coincides with the breakdown of the percolating network marked by the right border of the grey-shaded area in Figure 2. The reason for this correlation is that the tpb-length starts to decrease as soon as the bridges between Pt islands collapse. Secondly, the maximum value of the tpb-length scales inversely with film thickness. This correlation traces back to an increasing number of holes per unit area with decreasing film thickness. Thirdly, in case of a 50-nm thick Pt thin film on YSZ tape, the tpb-length can be adjusted between 0.3 μm^{-1} and 3.9 μm^{-1} by targeted adjustment of the agglomeration state (compare Figure 2). Accordingly, the maximum tpb-length is 13 times longer compared to the tpb-length of samples featuring the first occurrence of holes.

Electrochemical impedance spectroscopy was used to investigate the electrode performance of agglomerated Pt films with respect to the previously determined microscopic tpb-lengths per electrode area. An Arrhenius plot, showing the ASRs of initially 50-nm thick Pt films, is given in **Figure 3**A. The ASRs decreased exponentially with increasing temperature. No dependency of the activation energy on the tpb-length was found. The mean activation energies accounted for 1.0(2) eV and 0.4(2) eV within the temperature ranges of 350 to 500 °C and 250 to 350 °C, respectively. While the high temperature value corresponds well with literature data,[19,20] no activation energies for the temperature regime below 350 °C have been reported so far. The change in thermal activation at 350 °C might be attributed to a change of the rate limiting step for the oxygen reduction reaction or the full association of oxygen vacancies in YSZ at low temperatures.[21,22] In Figure 3B the corresponding electrode conductances $(ASR)^{-1}_{tot}$, which are the reciprocal ASRs, are plotted as a function of the microscopic tpb-length per electrode area for three operating temperatures. SEM top-view images of the corresponding Pt electrode morphologies are shown in Figure 3C. It follows in a first approximation that the conductance $(ASR)^{-1}_{tot}$ increases linearly with the tpb-length per electrode area. This is in agreement with literature.[10,16] However, it is interesting to note that the fitted lines do not extrapolate to the origin. This indicates that either the "dense" area of the Pt films shows appreciable electrochemical activity or that the geometrically derived microscopic tpb-length per electrode area is heavily underestimated.

2.2. The Role of "Nanoscopic" tpbs for the Electrode Performance of Pt Films

The electrochemical performance of Pt electrodes on YSZ was shown to scale linearly with the microscopic tpb-length per electrode area. Accordingly, a substantial increase of ASR was expected when comparing agglomerated Pt films featuring a clearly-defined microscopic tpb-length in the range of μm^{-1} to dense Pt films being either too thick to form holes during annealing (above 270 nm, compare Figure 1) or being in their as-deposited state. The microstructure of 50-nm thick Pt films as-sputtered on polycrystalline YSZ tape at 27 µbar and 360 W

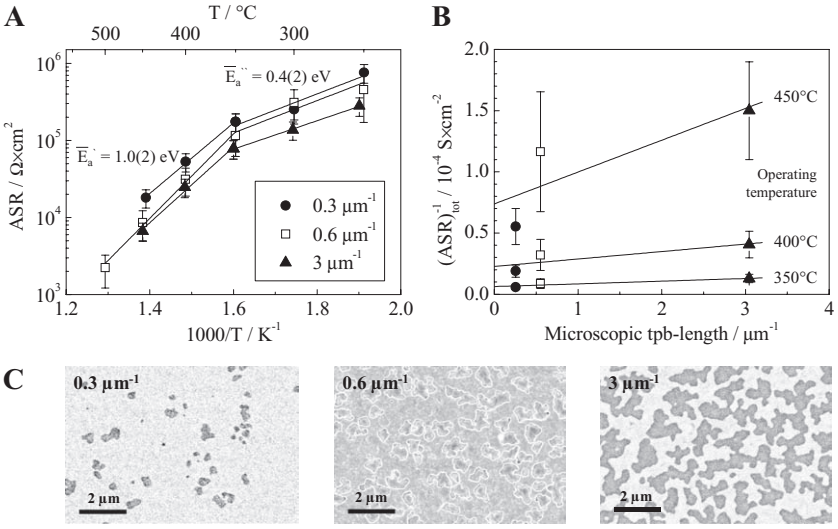

Figure 3. Electrode performance of initially 50-nm thick Pt films with respect to microscopic tpb-length per electrode area. Three different tpb-lengths of 0.3 μm^{-1}, 0.6 μm^{-1} and 3 μm^{-1} were obtained by annealing for 2 h at 625 °C, 650 °C or 675 °C, respectively. (A) Arrhenius plot of the ASR. (B) Total electrode conductance $(ASR)^{-1}_{tot}$ with respect to tpb-length and operating temperature. (C) Corresponding SEM images depicting the film morphologies and tpb-lengths. All films were deposited in 27 µbar of Ar using a plasma power of 360 W.

is illustrated in **Figure 4**. As shown in Figure 4A, the surface of as-deposited Pt films exhibited a granular structure with a feature size around 30 nm. In addition, a network of grooves with a characteristic diameter around 400 nm mirrored the subjacent grain boundaries of the polycrystalline YSZ substrate. In Figure 4B, a fractured cross-section of this Pt film peeled off from the YSZ tape is shown. It is recognizable that the as-deposited Pt thin films exhibited a predominantly columnar microstructure with a mean column diameter of 30 nm. Furthermore, the lower surface of the Pt thin film, formerly in contact with the YSZ tape, appears to be dense. It follows that the grooves on the surface of the Pt thin film did not penetrate the Pt film completely and reach the Pt | YSZ interface. A corresponding FIB-cut cross-section of the same film is shown in Figure 4C. The columnar Pt grains form a dense layer with predominantly vertically oriented grain boundaries. No delaminations or voids at the Pt | YSZ interface were found on several cuts adding up to a total length of more than 20 µm. The waviness of the Pt film corresponds to the grain size of the polycrystalline YSZ tape of 400 nm.

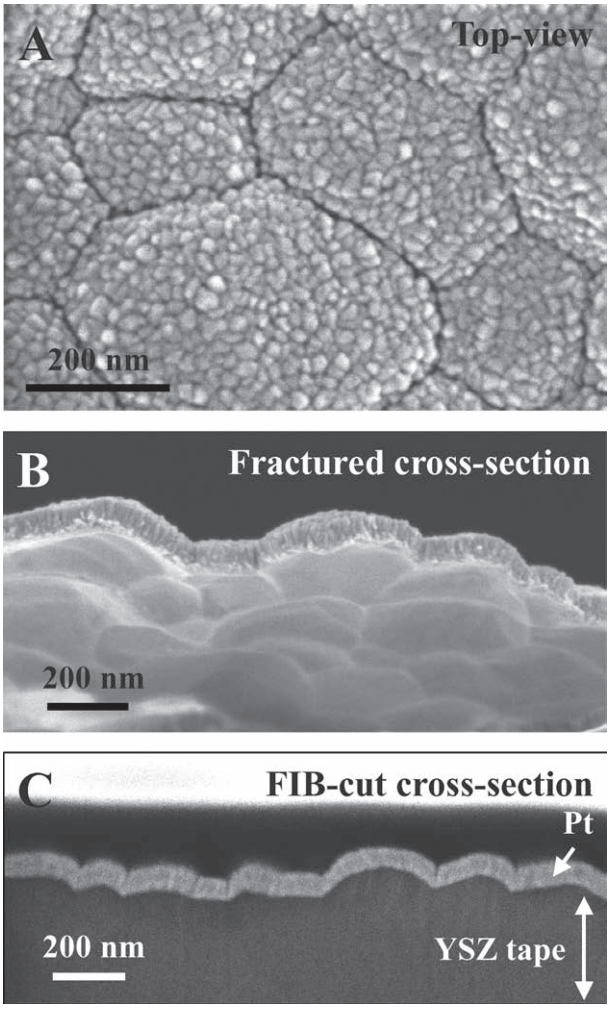

Figure 4. SEM images of 50-nm thick Pt films as-deposited on YSZ tape. (A) top-view. (B) fractured cross-section. (C) FIB-cut cross-section. The films were deposited in 27 µbar of Ar using a plasma power of 360 W.

In **Figure 5** the ASR of initially 50-nm thick, agglomerated Pt films with a microscopic tpb-length of 0.6 μm^{-1} is compared to 360-nm thick, annealed but dense Pt films as well as 50-nm thick, as-deposited and dense Pt films. Surprisingly, the as-deposited films without microscopic tpb showed a 4 times lower resistance than the agglomerated films with a microscopic tpb-length of 0.6 μm^{-1}. Furthermore, the ASR of the 360 -nm thick, annealed but dense Pt films without microscopic tpb was only slightly enhanced compared to the agglomerated films.

On the basis of the negligible solubility for oxygen in Pt we conclude that microstructural features like grain boundaries, triple lines, grain boundary grooves and voids act as "nanoscopic" tpbs and provide sufficiently fast reaction pathways for the incorporation of oxygen into the subjacent YSZ electrolyte. This holds true even in case of Pt films that do not feature any visible and defined microscopic tpb and are mostly regarded as "dense" in top-view SEM images. Literature reporting significant oxygen incorporation by diffusion of oxygen through the grain boundaries of Pt films substantiates this hypothesis.[23,24] We therefore propose Equation 1 describing the fact that the total conductance $(ASR)^{-1}_{tot}$ of Pt thin film electrodes is additively composed of a basic conductance due to "nanoscopic" tpbs $(ASR)^{-1}_{0}$ and a conductance due to the defined and "microscopic" tpbs, originating from agglomeration or micro-patterning $(ASR)^{-1}_{tpb}$. The basic conductance due to "nanoscopic" tpbs $(ASR)^{-1}_{0}$ remains available in dense films with zero "microscopic" tpb-length and depends strongly on the processing conditions, thickness and consequential microstructure.

$$(ASR)^{-1}_{tot} = (ASR)^{-1}_{0} + (ASR)^{-1}_{tpb} \quad (1)$$

Based on equation 1 the electrode conductance due to "microscopic" tpbs of the agglomerated and initially 50-nm thick Pt films $(ASR)^{-1}_{tpb}$ can be deduced from their total conductances $(ASR)^{-1}_{tot}$, presented in Figure 3B. Thereby, the total conductance of dense, 360-nm thick Pt films on YSZ tape, annealed at 650 °C for 2 h, is assumed to be a suitable approximation for the conductance due to "nanoscopic" tpb $(ASR)^{-1}_{0}$ of agglomerated Pt films. While the 360-nm thick films remained

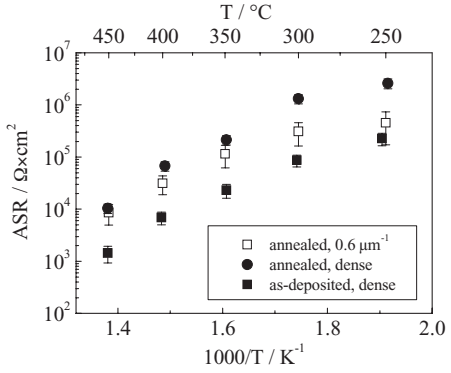

Figure 5. Electrode performance of agglomerated Pt films compared to dense films. The agglomerated films with a tpb-length per electrode area of 0.6 μm^{-1} were initially 50-nm thick and annealed for 2 h at 650 °C. The annealed but dense films were 360-nm thick and annealed at 650 °C for 2 h, as well. No annealing was applied in case of the as-deposited and dense films with a thickness of 50 nm. All films were deposited in 27 µbar of Ar using a plasma power of 360 W.

dense during annealing at 650 °C, the evolution of grain size was in a first approximation comparable to 50-nm thick films. In both cases the annealing resulted in a mean grain diameter around 100 nm. Accordingly, the electrode conductance tracing back to the "microscopic" tpbs in the 50-nm thick films $(ASR)^{-1}_{tpb}$ is calculated using equation 2. As the agglomerated electrodes did not cover the complete electrolyte area any more, the conductance $(ASR)^{-1}_0$ was multiplied by the area coverage *A*.

$$(ASR)^{-1}_{tpb} = (ASR)^{-1}_{tot} - [A \cdot (ASR)^{-1}_0] \quad (2)$$

The resulting $(ASR)^{-1}_{tpb}$ for agglomerated and initially 50-nm thick Pt films is plotted as a function of tpb-length for three operating temperatures in **Figure 6**. The fact that the linear fits nicely cross the origin is a clear indication that the total conductance of thin Pt films $(ASR)^{-1}_{tot}$ is indeed additively composed of a conductance due to "nanoscopic" tpb on Pt thin film areas mostly regarded as "dense" $(ASR)^{-1}_0$ and a conductance tracing back to the "microscopic" tpbs of agglomerated thin films visible in SEM images $(ASR)^{-1}_{tpb}$.

Scheme 1 illustrates the differentiation made between "microscopic" and "nanoscopic" tpbs in this study: (i) *"Microscopic tpbs"* result either from agglomeration during annealing (this study) or micro-patterning of Pt films. They can be determined geometrically by SEM image analysis and add up to tpb-lengths per electrode area in the range of μm^{-1}. (ii) *"Nanoscopic tpbs"* trace back to microstructural defects such as grain boundaries, grain boundary grooves and voids, and give rise to electrochemical activity even in case of thin Pt films commonly regarded as "dense". While the areal length of "nanoscopic" tpbs depends strongly on the processing conditions of thin Pt films, it potentially exceeds the tpb-length obtainable by "microscopic" tpbs by orders of magnitude.

In case of investigations using micro-patterned Pt films, the electrochemical activity due to "nanoscopic" tpbs $(ASR)^{-1}_0$ is easily accessible by electrochemical characterization of unpatterned films. During agglomeration of thin films at elevated temperatures, however, the formation of "microscopic" tpb and microstructural changes like grain growth take place simultaneously. Hence, the electrochemical activity $(ASR)^{-1}_0$ due to "nanoscopic" tpb in these films is not directly accessible.

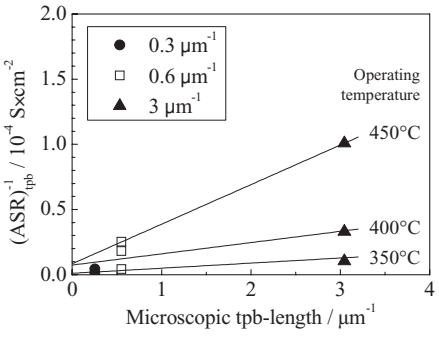

Figure 6. Electrode conductance $(ASR)^{-1}_{tpb}$, attributed to the microscopic tpb of agglomerated and initially 50-nm thick Pt films. Different tpb-lengths per electrode area were obtained by annealing for 2 h at 625, 650, or 675 °C. All films were deposited in 27 µbar of Ar using a plasma power of 360 W.

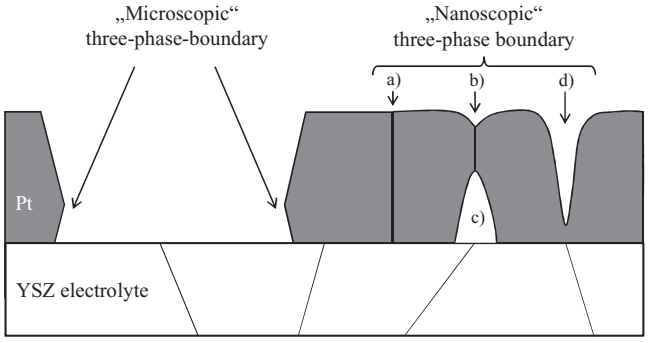

Scheme 1. Schematic illustration of nanoscopic and microscopic tpbs of thin Pt electrodes. a) Grain boundaries and triple lines, b) grain boundary grooves, c) voids, d) grooves above grain boundaries of the electrolyte.

2.3. Maximization of the "Nanoscopic" tpb-length by Adjustment of the Deposition Conditions

The electrochemical data presented in this study suggests that promoting "nanoscopic" grain boundaries is a more promising strategy in order to obtain high Pt electrode performances compared to an optimization of the "microscopic" tpb-length by agglomeration or micro-patterning. This has been demonstrated by the intrinsic electrochemical activity of "dense" Pt films in this study. Accordingly, thin film microstructures featuring extremely small grains, grain boundary grooving and nanoporosity are required. We approached the fabrication of thin Pt films with an augmented areal density of defects by an increase of the Ar pressure to 100 µbar and reduction of the plasma power to 100 W during sputtering. The resulting surface structure of a 50-nm thick film is shown in **Figure 7**A. The modified deposition conditions resulted in a high roughness and pronounced separation of the individual Pt features. The Pt feature size is around 30 nm and grooves reflect the YSZ grain boundaries. A fractured cross-section shown in Figure 7B reveals a network of voids at the lower side of the Pt film. Judging from the FIB cut cross-section shown in Figure 7C closed voids at the Pt | YSZ interface coexist with grooves reaching from the film surface to the electrolyte surface. Summing up, the modification of sputter parameters induced the formation of voids and grooves resulting in porosity in the nanometer range.

In **Figure 8** the ASR of originally 50-nm thick agglomerated Pt thin films annealed at 650 °C for 2 h is compared to the ASR of 50-nm thick, as-deposited films sputtered using two different sets of sputter parameters (27 µbar, 360 W or 100 µbar, 100 W). In addition, literature data for sputtered Pt electrodes on YSZ substrates is given. As-deposited Pt electrodes with a high concentration of microstructural defects, achieved by an increased sputtering pressure and decreased plasma power featured a reduced ASR approximately 1.5 orders of magnitude lower compared to the agglomerated film. A comparison with literature data reveals the high scatter spanning over eight orders of magnitude at 350 °C. This is partly caused by incommensurable lengths of the "nanoscopic" and "microscopic" tpbs due to various processing-conditions applied in the different studies. The high length of "nanoscopic" tpb in the as-deposited films presented in this study gives rise to a lower ASR compared to most literature reports. The very low ASR

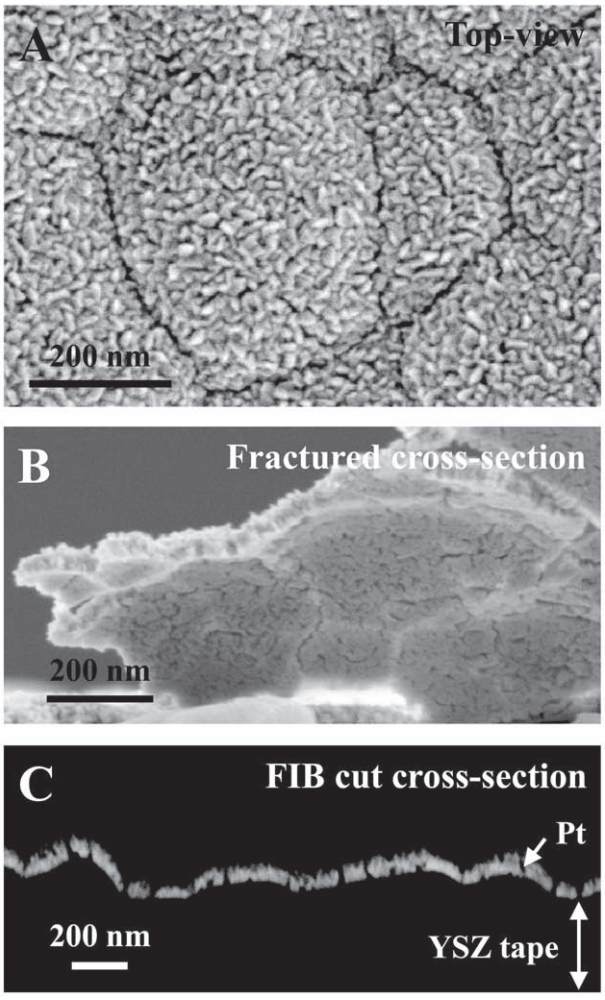

Figure 7. SEM images of 50-nm thick Pt films as-deposited on YSZ tape. (A) top-view. (B) fractured cross-section. (C) FIB-cut cross-section. The films were deposited in 100 µbar of Ar using a plasma power of 100 W.

of approximately 30 Ω cm^2 measured by Huang et al. at open circuit voltage for SOFCs consisting of a 50-nm thick YSZ electrolyte sandwiched between 80-nm thick Pt electrodes, might trace back to the nano-crystallinity of the YSZ electrolyte enhancing the oxygen incorporation in addition to the electrochemically active electrodes.

Literature points at a detrimental effect of Si impurities on the performance of Pt electrodes.[25] However, an influence of changing impurity concentrations on the effects observed in this study can be ruled out a priori for all experiments where solely the change of sputtering conditions resulted in a variation of the ASR of as-deposited Pt films. Annealed Pt films on YSZ tape were subjected to additional XPS analysis. This confirmed that the Si contamination on the YSZ tape used in this study was close to the XPS detection limit and the amount of Si on the YSZ surface did not change during annealing up to 675 °C. Therefore, the differences in electrochemical activity observed in this study are attributed to changes in the areal lengths of "microscopic" and "nanoscopic" tpbs only. However, a quantitative comparison of impurity concentrations between different studies is difficult.

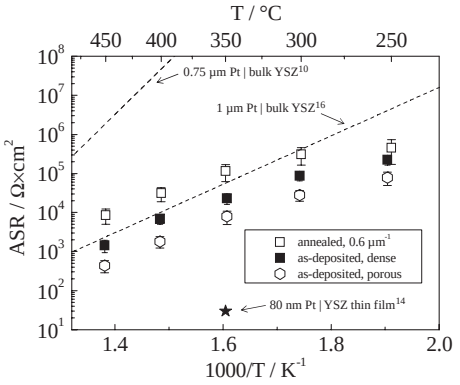

Figure 8. Electrode performance of initially 50-nm thick Pt films with respect to temperature. Annealed films with a microscopic tpb-length per electrode area of 0.6 µm^{-1} are compared to films, as-deposited using two different sets of sputtering conditions (27 µbar and 360 W or 100 µbar and 100 W). Literature data for Pt films on YSZ is shown as well.

Besides differences in tpb-lenghts impurities may also contribute to the large scatter of ASR data available in literature.

With respect to the application of Pt electrode thin films in electrochemical devices this study demonstrates that targeted agglomeration and adjustment of tpb-lengths is useful to fabricate reasonably well-performing electrodes that do not undergo microstructural changes during application at temperatures below the agglomeration temperature. However, providing high areal lengths of "nanoscopic" tpbs by low grain sizes, grain boundary grooving and void formation during thin film deposition is the way to go in order to maximize the performance of thin Pt electrodes. Furthermore, the impact of the defect concentration of the underlying electrolyte on the Pt electrode performance requires additional attention in the future.

3. Conclusions

The agglomeration of thin Pt films on polycrystalline YSZ tape during annealing proceeds faster the thinner the film and the higher the temperature is. By targeted choice of the annealing conditions thin film morphologies ranging from dense Pt films over two-dimensionally percolating Pt networks with defined tpb-length to isolated Pt particles can be obtained. After annealing for 2 h at 650 or 800 °C, 180 nm or 380 nm of film thickness, respectively, are required in order to avoid the formation of open porosity. In order to maintain percolating Pt networks at these two temperatures minimum film thicknesses of 50 or 145 nm are needed (compare Figure 1). The maximum microscopic tpb-length per unit area of agglomerated Pt films derived from top-view SEM images scales inversely with the film thickness prior to annealing. In case of a 50-nm thick Pt films a maximum microscopic tpb-length per electrode area of 3.9 µm^{-1} was obtained. Such high microscopic tpb-lengths are hardly feasible by micro-patterning techniques.

The conductance of agglomerated Pt thin film electrodes on polycrystalline YSZ tape was found to scale linearly with the microscopic tpb-length per electrode area. However, dense Pt films showed significant electrochemical activity as well. We, therefore, postulate that the total conductance $(ASR)^{-1}_{tot}$

of thin Pt electrodes on YSZ tape is additively composed of a conductance tracing back to "nanoscopic" tpb provided by grain boundaries, triple lines, grain boundary grooves and voids and a conductance due to the defined and easily measurable "microscopic" tpb available in case of agglomerated or micro-patterned thin films. The conductance due to "nanoscopic" tpb depends strongly on the microstructure of Pt films and can even outweigh the conductance due to microscopic tpb. Accordingly, Pt films commonly regarded as "dense" are capable of featuring high electrochemical activities, excelling agglomerated or micro-patterned films by far.

In view of electrode applications these results imply that the state-of-the-art picture of a microscopic and geometrically measurable tpb providing the performance of Pt thin film electrodes is obsolete. It is rather the nanostructure involving grain boundaries, triple lines, grooves and voids, which determines the ASR of Pt thin films on YSZ. Hence, intelligent tailoring of the nanostructure of metal electrodes will be the key to superior Pt electrode performances in the future. However, the reduction of grain and feature sizes might impair the thermal stability of highly active metallic thin film electrodes. This will be subject of further studies.

4. Experimental Section

Thin film processing: 150 µm thick, polycrystalline $(ZrO_2)_{0.92}(Y_2O_3)_{0.08}$ (YSZ) tape (Kerafol, Germany) with a grain size in the range of 0.4 µm was used as substrate. Prior to Pt deposition the tape was cleaned by acetone and 2-propanol in an ultrasonic bath and rinsed in ultrapure water.

Pt thin films with thicknesses in the range of 15 to 360 nm were deposited on YSZ tape by DC magnetron sputtering using a PVD Products system. The target (purity > 99.99 at.%, Sindlhauser Materials, Germany) with a diameter of 76 mm was located at a target-substrate distance of 160 mm and exhibited a tilt angle of 35° relative to the substrate. After pumping to a base pressure of 10^{-9} bar, the depositions were carried out in 27 µbar of Ar (purity > 99.998%, PanGas, Switzerland), at 360 W and room temperature. These sputter conditions yielded a deposition rate of 1.14 nm/s. For comparison a few Pt films were deposited at a higher Ar pressure of 100 µbar and a lower plasma power of 100 W. During depositions the substrate was rotated to guarantee a homogeneous distribution of film thickness.

After thin film deposition the YSZ tapes coated with Pt at 27 µbar and 360 W, were annealed in air for 2 h (muffle furnace Nabertherm L3/11/P320, Germany) at temperatures between 625 and 800 °C. This temperature range was chosen to be clearly separated from the temperature range of electrochemical characterization (250–500 °C) in order to avoid simultaneous morphological changes. Pt films deposited in 100 µbar of Ar at a plasma power of 100 W were characterized in the as-deposited state only.

Microstructural characterization: A Leo 1530 (Carl Zeiss SMT, Germany) scanning electron microscope (SEM) was used for the characterization of thin films with respect to film thickness, morphology and microstructure. Overview images were taken by the in-lens detector at an acceleration voltage of 3 kV. For quantitative analysis of agglomeration patterns a four-quadrant backscattered electron detector (4QBSD) was used rendering images with a high material contrast between Pt and the YSZ substrate. At least six images per sample were taken at the highest available resolution using a magnification leading to a statistically significant amount of Pt features on the images. For image analysis Image J 2.1.6.3 (Wayne Rasband, National Institutes of Health, USA) and IgorPro 6.0 (WaveMetrics, USA) were used. Quantitative measures following from this analysis comprised the substrate area uncovered during the agglomeration process as well as the resulting "microscopic" tpb-length per electrode area. The error estimation regarding these two parameters was based on the addition as well as subtraction of two pixels to the diameter of the Pt features and respective recalculation of both values. The continuity of agglomerated Pt-networks was tested by contacting the film surface with the two probes of a handheld multimeter. Cross-sections were cut, polished and imaged by a NVISION 40 focused ion beam (FIB) workstation (Zeiss, Germany).

Electrochemical characterization: For the electrochemical characterization of Pt thin films symmetrical cells were fabricated by the deposition of Pt on both sides of the YSZ substrate. A sketch of the sample design is shown in **Scheme 2**. Uniform and reproducible contacting was assured by deposition of 500-nm thick Au frames overlapping all four edges of the Pt electrodes. The Au frames were sputtered within 4 min with 60 mA at 50 µbar and a target-substrate distance of 6 cm in a SCD 050 sputter coater (Bal-tec, Liechtenstein). Flattened Pt wires were attached to the Au surface by Au paste (C 5754 B, Heraeus, Germany) and ceramic glue (Feuerfestkitt, Firag, Switzerland).

A tube furnace (Gero, Germany) constantly flushed by 50 mL/min of humidified air was used for electrochemical characterization. Measurements were done during stepwise cooling from the maximum temperature. At each temperature step 10 min were awaited isothermally in order to let the sample equilibrate. In order to monitor the temperature a type K thermocouple (Omega Engineering, USA) was placed next to the sample. Impedance spectra of the symmetrical cells were recorded by a Solartron 1260 impedance analyzer (Solartron Analytical, UK), operated between 10 mHz and 4 MHz using an oscillation amplitude of 20 mV. A typical impedance spectrum measured at 350 °C on an initially 50-nm thick Pt film on YSZ tape annealed at 650 °C for 2 h is shown in **Figure 9**A. Three semicircles I–III can be distinguished. When the temperature exceeded 400 °C, two semicircles remained only. The impedance data was fitted to the equivalent circuit shown in Figure 9B using ZView (Scribner Associates, USA). According to the number of observed semicircles the parallel connection of an ohmic resistor and a constant phase element (CPE) -R2-CPE2- was not applied for spectra measured above 400 °C. The assignment of physical processes to the semicircles I-III was done on the basis of their relaxation times τ. These were calculated from the parameters of R-CPE elements using equation 3, given that the relaxation time is the reciprocal of the angular frequency at the maximum of the Nyquist diagrams ω.[26] Q and n refer to the pre-factor and the exponent of the CPE in parallel with the ohmic resistance R.

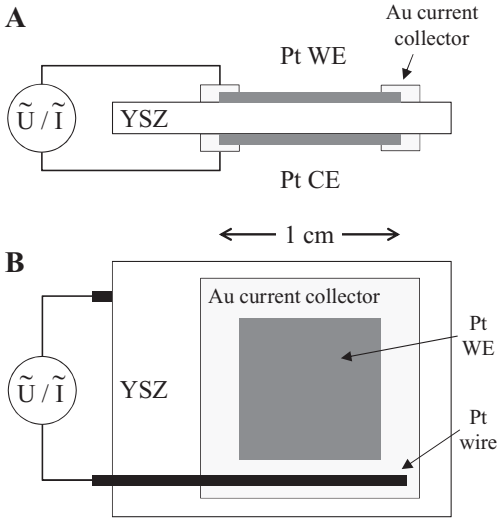

Scheme 2. Scheme of a symmetrical cell used for the electrochemical characterization of thin Pt films on YSZ – (A) cross-section, (B) top-view.

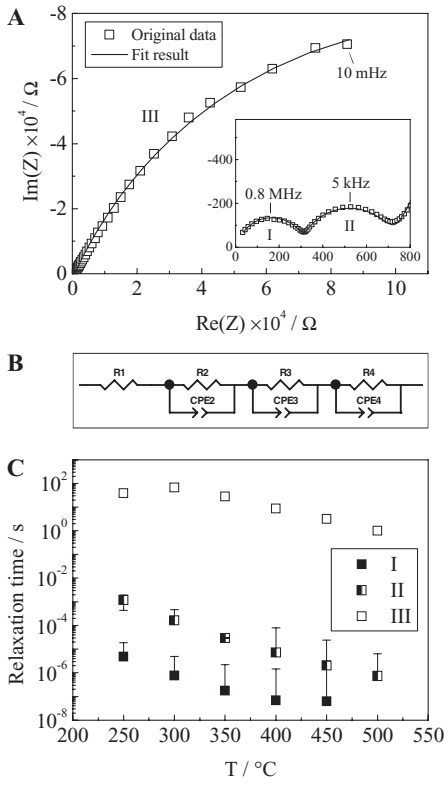

Figure 9. (A) Typical impedance spectrum of agglomerated Pt films (initial thickness: 50 nm, annealing: 650 °C for 2 h) on YSZ tape measured at 350 °. Three semicircles can be distinguished (I-III). (B) Equivalent circuit used for the fitting of impedance data. The element -R2-CPE2- was applied below 450 °C only. (C) Relaxation times of the processes I-III plotted as a function of temperature.

$$t = (Q \cdot R)^{(1/n)} \tag{3}$$

The relaxation times of the semicircles I-III are plotted in Figure 9C as a function of temperature. While the relaxation times decrease exponentially with increasing temperature, they clearly differ in their magnitude, which is 0.06 µs and 6 µs for the high and middle frequency semicircle and 14 s for the low frequency semicircle at 400 °C. Accordingly, the high and middle frequency semicircles I and II were ascribed to the bulk and grain boundary impedance of the polycrystalline YSZ electrolyte, respectively. The low-frequency semicircle III was attributed to the electrode process. [2,11,20,25,27,28] Therefore, the ohmic resistance of the third semicircle R_{III} corresponded to the electrode polarization resistance.

As symmetrical cells were used, only half of the electrode polarization resistance allotted to one electrode. Area specific resistances (ASRs) were obtained by multiplication of half of the electrode polarization resistance R_{III} by the electrode area unsealed by the Au grid. The error estimation concerning ASR values was based on a maximum systematic error of 0.2 cm^2 with respect to the electrode area as well as a statistical error that was assessed by the characterization of at least two identical samples.

Acknowledgements

Financial support by the following Swiss institutions is gratefully acknowledged:

- Competence Centre for Materials Science and Technology (CCMX) within the framework of the NANCER project
- Center of Competence Energy and Mobility (CCEM) within the framework of the ONEBAT project
- Swiss Electric Research (SER) within the framework of the ONEBAT project
- Swiss National Foundation (SNF) within the framework of Sinergia project ONEBAT

Furthermore, the authors want to thank Prof. Janek of the Justus Liebig University Giessen and Prof. Fleig of the Vienna University of Technology for advice and fruitful discussions. Thomas Ryll is indepted to Meike Schlupp from the Nonmetallic Inorganic Materials group, ETH Zurich, for XPS analysis and Michael Schinhammer from the Laboratory of Metal Physics and Technology, ETH Zurich, for assistance with SEM imaging.

Received: August 20, 2010
Published online: December 6, 2010

[1] A. Mitterdorfer, L. J. Gauckler, *Solid State Ionics* **1999**, *117*, 187.
[2] A. Mitterdorfer, L. J. Gauckler, *Solid State Ionics* **1999**, *117*, 203.
[3] A. Mitterdorfer, L. J. Gauckler, *Solid State Ionics* **1999**, *120*, 211.
[4] R. Radhakrishnan, A. V. Virkar, S. C. Singhal, G. C. Dunham, O. A. Marina, *Sens. Actuators B* **2005**, *105*, 312.
[5] A. Evans, A. Bieberle-Hütter, J. L. M. Rupp, L. J. Gauckler, *J. Power Sources* **2009**, *194*, 119.
[6] N. L. Robertson, J. N. Michaels, *J. Electrochem. Soc.* **1990**, *137*, 129.
[7] D. J. Srolovitz, M. G. Goldiner, *JOM* **1995**, *47*, 31.
[8] N. Baumann, E. Mutoro, J. Janek, *Solid State Ionics* **2010**, *181*, 7.
[9] R. H. Brandon, F. J. Bradshaw, *Royal Aircraft Establishment Research Report* **1966**, *No. 66095*.
[10] M. J. Verkerk, M. W. J. Hammink, A. J. Burggraaf, *J. Electrochem. Soc.* **1983**, *130*, 70.
[11] M. J. Verkerk, A. J. Burggraaf, *J. Electrochem. Soc.* **1983**, *130*, 78.
[12] A. J. A. Winnubst, A. H. A. Scharenborg, A. J. Burggraaf, *Solid State Ionics* **1984**, *14*, 319.
[13] U. P. Muecke, D. Beckel, A. Bernard, A. Bieberle-Hutter, S. Graf, A. Infortuna, P. Muller, J. L. M. Rupp, J. Schneider, L. J. Gauckler, *Adv. Funct. Mater.* **2008**, *18*, 3158.
[14] H. Huang, M. Nakamura, P. Su, R. Fasching, Y. Saito, F.B. Prinz, *J. Electrochem. Soc.* **2007**, *154*, B20.
[15] X. Wang, H. Huang, T. Holme, X. Tian, F. B. Prinz, *J. Power Sources* **2008**, *175*, 75.
[16] R. Radhakrishnan, A. V. Virkar, S. C. Singhal, *J. Electrochem. Soc.* **2005**, *152*, A927.
[17] W. C. Maskell, N. M. Sammes, B. C. H. Steele, *J. Phys. D: Appl. Phys.* **1987**, *20*, 99.
[18] T. J. Coutts, B. Hopewell, *Thin Solid Films* **1972**, *9*, 37.
[19] D. Y. Wang, *J. Electrochem. Soc.* **1990**, *137*, 3660.
[20] D. E. Vladikova, Z. B. Stoynov, A. Barbucci, M. Viviani, P. Carpanese, J. A. Kilner, S. J. Skinner, R. Rudkin, *Electrochim. Acta* **2008**, *53*, 7491.
[21] J. D. Solier, I. Cachadina, A. Dominguezrodriguez, *Phys. Rev. B* **1993**, *48*, 3704.
[22] C. Leon, M. L. Lucia, J. Santamaria, *Phys. Rev. B* **1997**, *55*, 882.
[23] R. Schmiedl, V. Demuth, P. Lahnor, H. Godehardt, Y. Bodschwinna, C. Harder, L. Hammer, H. P. Strunk, M. Schulz, K. Heinz, *Appl. Phys. A: Mater. Sci. Proc.* **1996**, *62*, 223.
[24] K. Sreenivas, I. Reaney, T. Maeder, N. Setter, C. Jagadish, R. G. Elliman, *J. Appl. Phys.* **1994**, *75*, 232.
[25] J. L. Hertz, A. Rothschild, H. L. Tuller, *J. Electroceram.* **2009**, *22*, 428.
[26] M. R. S. Abouzari, F. Berkemeier, G. Schmitz, D. Wilmer, *Solid State Ionics* **2009**, *180*, 922.
[27] J. E. Bauerle, *J. Phys. Chem. Solids* **1969**, *30*, 2657.
[28] J. Mizusaki, K. Amano, S. Yamauchi, K. Fueki, *Solid State Ionics* **1987**, *22*, 323.